Ultrasonics 131 (2023) 106945

Contents lists available at ScienceDirect

Ultrasonics

journal homepage: www.elsevier.com/locate/ultras

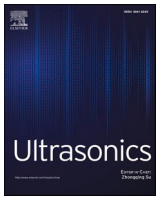

In situ nonlinear Rayleigh wave technique to characterize the tensile plastic deformation of stainless steel 316L

Changgong Kim *, Kathryn H. Matlack

Department of Mechanical Science and Engineering, University of Illinois at Urbana-Champaign, Urbana, IL 61801, USA

ARTICLE INFO

Keywords:
Nonlinear ultrasound
Rayleigh wave
Acoustic nonlinearity parameter
Plastic deformation
In situ measurements

ABSTRACT

The acoustic nonlinearity parameter β is sensitive to dislocation parameters, which continuously change during plastic deformation. Dislocation-based damage in structures/components is the source of the failure; thus, β has been studied as a metric for non-destructive evaluation. This work consists of two parts: the development of an in situ experimental setup for nonlinear Rayleigh wave measurements, and characterization of the dependence of β on applied stress at different levels of initial plastic strain. First, we introduce an experimental setup and methods for repeatable in situ nonlinear ultrasonic measurements. Details on design considerations and measurement schemes are provided. In the second part, β was measured in situ during an incremental monotonic tensile test. The measured β monotonically decreases with plastic strain, but it is relatively insensitive to the applied stress during elastic deformation. This result highlights three aspects of the evolution of β, which have not been sufficiently emphasized in prior work: the apparent insensitivity of β to the applied stress during elastic deformation, decreasing β with plastic deformation, and the saturation of β. We attribute the trend of decreasing β to a scaling of β with monopole loop length during plastic deformation, which depends on initial microstructure. The saturation of β at 1.8% coincides with a planar-to-wavy transition of dislocation structures. The in situ nonlinear ultrasonic experimental method presented in this work is significant as the in situ results can provide broader insights on β and dislocation-based damage evolution than ex situ measurements alone.

1. Introduction

When materials plastically deform, dislocations are generated to accommodate the imposed damage. As the damage accumulates, the number density of dislocations increases, and they evolve into more complex but organized configurations. Nonlinear ultrasound (NLU) is sensitive to the changes in dislocation structures, which enables the nondestructive evaluation of dislocation-based damage by measuring the nonlinear ultrasonic response of dislocations. The acoustic nonlinearity parameter β is often used to quantify the nonlinearity of dislocation motions. The nonlinearity of dislocations depends on dislocation parameters, which continuously change during damage accumulation regardless of the damage mechanisms. Thus, the sensitivity of the NLU technique to dislocation parameters makes it a potentially useful NDE tool for monitoring structures/components exposed to dislocation-based damage.

According to the theoretical models, β depends on material constants, internal stress, and dislocation parameters, e.g., dislocation density, monopole loop length, and dipole height [1–4]. The dependence of β on dislocation parameters has been extensively studied for damage mechanisms such as monotonic tension [5,6], fatigue [2,5,7], and precipitation [8,9]. The results reported in the prior work confirm that the evolution of β correlates to the changes in dislocation parameters. However, there has been little work on the effect of internal stress on β. While Shui et al. measured β as a function of the applied stress during monotonic tension tests [10], the effect of the applied stress was not discussed in detail.

Cash et al. were the first who highlighted the significance of the internal stress [4]. They updated Cantrell's models [2] to include the stress-dependence of β, and their models highlight two aspects of the evolution of β during plastic deformation: the possibility of negative β and the dependence of β on the internal stress and dislocation configurations. Recently, Gao et al. also developed a dislocation pile-up model that predicts negative β [11].The negative contribution to β is especially noteworthy since it can cancel out positive contributions and underestimates β. The significance of negative β is that the measured β can decrease with damage accumulation, which contrasts with typical findings in prior work: a monotonic increase in β with damage

* Corresponding author.
E-mail address: ckim130@illinois.edu (C. Kim).

https://doi.org/10.1016/j.ultras.2023.106945
Received 26 April 2022; Received in revised form 27 October 2022; Accepted 31 January 2023
Available online 4 February 2023

accumulation. However, the decrease in β during plastic deformation has been rarely reported.

The stress dependence of β can be experimentally studied using in situ NLU measurements. The in situ NLU measurements allow to change the stress term while keeping other model parameters constant. There is a few work on in situ NLU measurements. For example, Shui et al. [10] made in situ β measurements using longitudinal waves on AZ31 Mg-Al alloy and Kim et al. [12,13] used Rayleigh waves to measure the dependence of β on creep and cyclic loading of concrete. However, prior work does not highlight the subject of this work: in situ setup, measurement procedures, and, above all, the dependence of β on the applied stress.

The first goal of this work is to develop in situ Rayleigh wave measurement fixtures and procedures for repeatable β measurements while a specimen is loaded. Compared to longitudinal wave measurements, nonlinear Rayleigh wave measurements can be more sensitive to the setup because the propagating wave transmits through multiple interfaces, e.g., transducer to wedge and wedge to the material. Further, in situ measurements during mechanical testing requires special considerations since measurements are done while a specimen is vertically mounted in the load frame. In the first part of work, we introduce in situ setup and measurement procedures for repeatable in situ NLU measurements. With custom-made fixtures, we achieved highly repeatable β measurements compared to those in the work of Shui et al. [10] and Kim et al. [12].

The second goal of this work is to characterize the dependence of β on applied stress in the elastic and plastic regimes, using our in situ nonlinear Rayleigh wave measurement setup. Our setup allowed accurate measurements of small changes to β as a function of the applied stress. The results highlight three aspects of the evolution of β in stainless steel (SS) 316L, which have not yet been shown in prior work: β is relatively insensitive to the applied stress during elastic deformation, β can decrease with increasing plastic strain, and β saturates with increasing plastic strain. Detailed discussions are provided to interpret these results in terms of dislocation structure evolution in stainless steel 316L under tensile loads.

2. Sample preparation and mechanical test

The as-received material was hot-rolled at 1100C and water-quenched for cooling. The as-received stainless steel 316L block was machined into a dog bone specimen with electrical discharge machining (EDM). The yield stress of the as-received material was 425 MPa. To reduce the yield stress to a similar level (~220 MPa) reported in prior work [14,15], the material was heat-treated for solution annealing at 1100C for 1 h, followed by water quenching to homogenize grains and minimize residual stress from hot working. The specimen surface was prepared by mechanically grinding the oxide layer with sandpaper of up to 2000grit for a smooth surface to improve the signal-to-noise ratio (SNR) of ultrasonic measurements.

The specimen was incrementally loaded up to 6.0 % total strain in stress control using the strain rate of 0.001 s^{-1}. The loading paths and the material behavior are provided in Fig. 1: The sample was first loaded to 0.72 % plastic strain, then unloaded to 0 MPa, then loaded to 1.3 % plastic strain, then unloaded, and this was repeated at 3.0 % and 5.7 % strain. Note that the unloading portion of the stress–strain curve is not plotted. The 0.2 % yield stress of the material is 225 MPa, and Young's modulus is 200GPa. The tensile test was interrupted at each data point in Fig. 1 to hold the specimen at fixed stress levels for ultrasonic measurements. The markers in Fig. 1 represents the stress and the strain conditions where ultrasonic measurements were made.

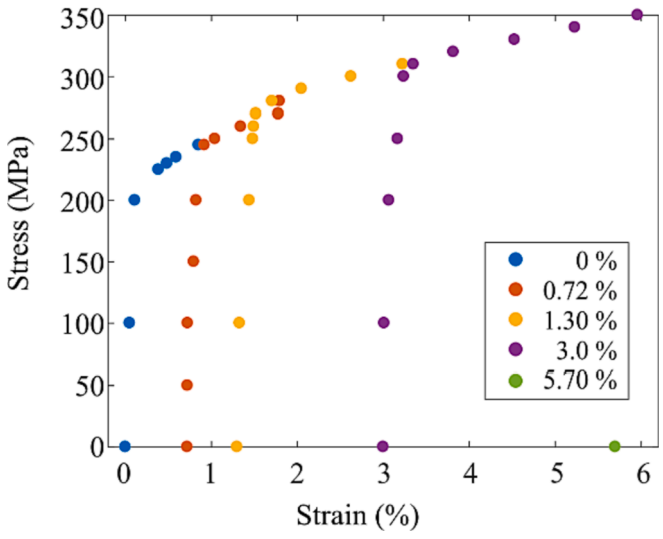

Fig. 1. A stress–strain curve of the tested SS 316L specimen. The loading history consists of 4 segments, starting at a different plastic strain as noted in the legend. The markers represent where ultrasonic measurements were made. β was measured three times when the applied stress is zero and only once when the applied stress is present.

3. In situ nonlinear Rayleigh wave measurements

3.1. Overview and background of NLU

NLU is a technique to measure material nonlinearity. When an ultrasonic wave of a fundamental frequency (f) propagates through a material with defects, a portion of its energy transfers to the second harmonic ($2f$) due to the nonlinear stress–strain response. The acoustic nonlinearity parameter β is a metric that quantifies the nonlinear ultrasonic response of defects. The relation between β and the Rayleigh wave parameters is:

$$\beta^{rayleigh} = \frac{u_2}{xu_1^2}\frac{i8\sqrt{k_R^2 - k_L^2}}{k_L^2 k_R}\left(1 - \frac{2k_R^2}{2k_R^2 - k_S^2}\right), \tag{1}$$

where u_1 and u_2 are the vibration displacement amplitudes of the first (f) and the second ($2f$) harmonics respectively and x is the propagation distance. The other variables are the wavenumber for a longitudinal wave (k_L), a shear wave (k_S), and a Rayleigh wave (k_R).

A relative acoustic nonlinearity parameter, β^{rel}, can be measured experimentally in two ways, as either.

$$\beta_{dist}^{rel} \propto \frac{A_2}{xA_1^2} \; or \; \beta_{amp}^{rel} \propto \frac{A_2}{A_1^2}, \tag{2}$$

where β_{dist}^{rel} is used for distance sweep (i.e., A_1 is fixed) and β_{amp}^{rel} is for amplitude sweep (i.e., x is fixed). Here, A_1 and A_2 are the measured amplitudes corresponding to f and $2f$ respectively. In this work, we used amplitude sweep for measurements and the detail is discussed in section 3.2. From here on, we use β to refer to β_{amp}^{rel}.

The measured nonlinearity is a sum of the intrinsic material nonlinearity β^{lat} and the nonlinearity of defects β^{def}, i.e., $\beta = \beta^{lat} + \beta^{def}$. The first term, β^{lat}, is defined as $\beta^{lat} = A_{111}/A_{11}$, where A is the Huang's coefficients written in Voigt notation, and remains almost constant during plastic deformation [16]. The second term, β^{def}, which is the excess nonlinearity due to defects such as dislocations, continuously change during plastic deformation; thus, β is used as a metric to evaluate the accumulation of dislocation-based damage.

The dislocation contributions to β^{def} depend on the geometric

configuration of dislocations, e.g., monopoles and dipoles. The models developed in prior work [2–4] have similar forms as shown in Eq. (3) and Eq. (4).

$$\beta_{mono}^{def}/\Lambda_{mono}b^2 = f_1(\nu)g_1(\Omega,R^3)\left(\frac{L}{b}\right)^4\left(\frac{\sigma}{\mu}\right) \tag{3}$$

$$\beta_{di}^{def}/\Lambda_{di}b^2 = f_2(\nu)g_2(\Omega,R^2)\left(\frac{h}{b}\right)^3 + f_3(\nu)g_3(\Omega,R^3)\left(\frac{h}{b}\right)^4\left(\frac{\sigma}{\mu}\right) \tag{4}$$

Here, subscript *mono* and *di* represent dislocation monopoles and dipoles respectively. The material constants such as Poisson's ratio (ν), burgers vector (b), orientation factors (Ω and R), and shear modulus (μ) are invariant during plastic deformation. L and h are monopole loop length and dipole height and Λ is dislocation density. Finally, σ is the internal stress acting on dislocations.

These equations readily show that both dislocation monopoles and dipoles have a linear dependence on the internal stress and that dislocation dipoles have an additional stress-independent term. In prior work, the internal stress term was accounted for in two different ways. Cantrell [2,17] and Apple [18] used the composite model of Mughrabi [19] and the endurance limit stress (the stress below which materials do not fail) to estimate the local stress state of dislocation substructures. In this approach, the internal stress evolution during plastic deformation is driven by the formation of veins and persistent slip bands (PSBs). The second approach uses the average residual stress from dislocation pile-ups to approximate the internal stress acting on dislocation substructures [20,21]. Compared to the first approach, the second approach is more useful for the planar slip metals, where veins and PSBs are hard to develop.

The internal stress calculated using two approaches is back stress generated by specific dislocation configurations. The applied stress in the macroscopic stress–strain curve is a sum of the frictional stress and the back stress [22,23]. The frictional stress represents the local resistance of the lattice to dislocation motions due to short-range interactions of dislocations. The back stress is induced by the long-range elastic interactions among dislocations due to grains and stress fields of dislocations. The evolution of the back stress depends on the number density of dislocations, which usually increases with plastic deformation. The advantage of using the back stress is that it relates to the macroscopic stress–strain curve. Thus, one can study the stress dependence of β by changing the applied stress and measuring β in situ during loading.

3.2. In situ measurement setup and method

We used a contact transducer of a 0.5″ diameter as a transmitter (Lithium Niobate transducer, NdtXducer, Northborough MA, USA) and an air-coupled transducer (ACT) as a receiver (Air-coupled transducer, Ultran group, State College PA, USA). A sinusoidal burst of 40 cycles tuned to the center frequency of the transmitter (2.075 MHz) was excited with a high-power amplifier (Ritec RAM-5000 SNAP, RITEC Inc., Warwick RI, USA) into the transmitter. The signal collected by the receiver was amplified into 30 dB with a pre-amplifier. Fig. 2 (a) shows the measurement configuration, and Fig. 2(b) shows the specimen after mounting ultrasonic fixtures and transducers. The representative time-domain signal is given in Fig. 3(a). The steady-state portion of the received signal was windowed with a Hanning window for FFT to extract the amplitude of the first (2.075 MHz) and the second (4.15 MHz) harmonics. The slope of A_2/A_1^2 is calculated as β (Fig. 3(b)), and the same measurements were repeated three times to get the standard deviation of measurements. Specifically, β was measured three times when the applied stress was zero and only once when the applied stress was non-zero.

As shown in Fig. 3(b), we used amplitude sweep in this work instead of distance sweep, which is more common [5,24], to calculate β when using Rayleigh waves. The advantage of distance sweep is that the system nonlinearity (e.g., nonlinearity generated from a transmitting transducer and coupling) can be isolated since the output of the high-power amplifier is fixed [25]. As shown by Torello et al. [26], system nonlinearity can be accounted for to prevent overestimation or underestimation of β. The details on the analytical method for isolation of system nonlinearity are given in Torello et al. [26]. However, distance sweep is sometimes not desirable if the geometry of the test specimen cannot be assumed as ideal, i.e., an infinite elastic half space. A few examples include geometries such as a curved surface [27,28] and a narrow dog-bone specimen [24]. For curved surfaces, a measurement variation is mainly due to the time-varying coupling of the wedge-specimen interface and difficulty with controlling the coupling layer [27]. In the case of a dog-bone geometry, the gauge width is usually comparable to the width of the effective line source (i.e., the wedge front). The boundary effect from the specimen is noted by Herrmann et al. [5], but currently, there is no available model to account for this phenomenon. In our preliminary measurements using distance sweep, we observed a periodic fluctuation of A_1 with a propagation distance, which significantly distorts the slope of the A_2/A_1^2 vs x. For amplitude

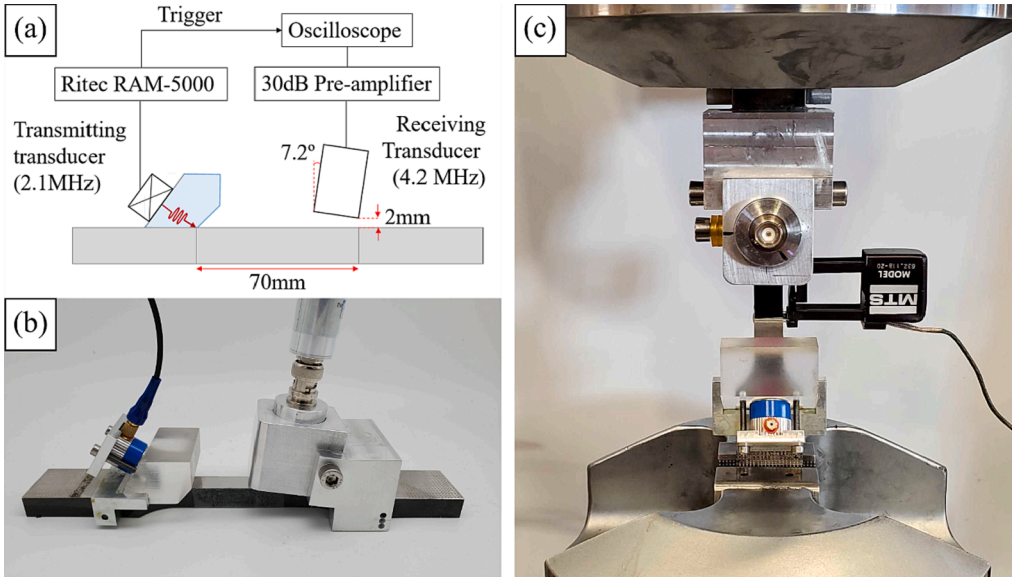

Fig. 2. (a) In situ NLU Rayleigh wave measurement schematic. The Rayleigh wave generated by the contact transmitting transducer interacts with all the dislocation substructures in the entire gauge length (70 mm) before it is collected by the air-coupled transducer. (b) The fixtures holding the wedge and the air-coupled transducer are glued to the specimen using silicone rubber. Note that the fixtures and the wedge are positioned outside the gauge length to prevent debonding during deformation. (c) The in situ measurement setup in the load frame. All the attachments remain mounted during in situ measurements except the wedge. The extensometer is mounted on the side of the specimen.

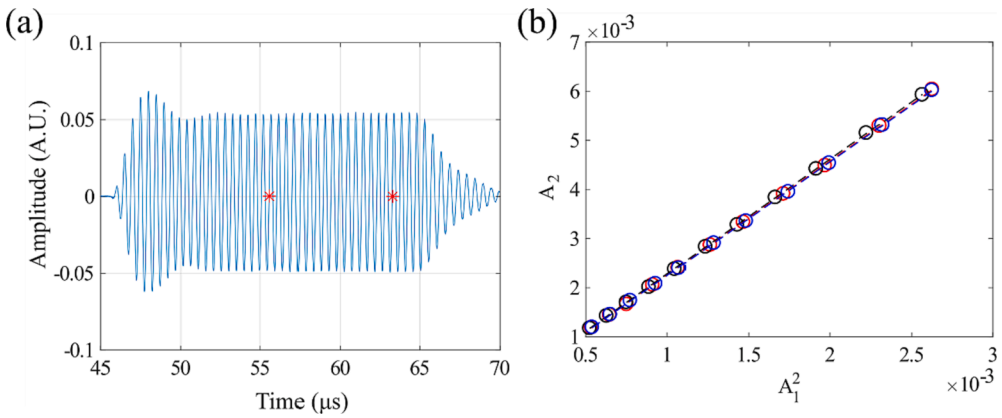

Fig. 3. (a) A representative time domain signal. A sinusoidal burst of 2.075 MHz was excited and the steady-state portion of the signal marked with red stars was used for post-processing to extract the amplitude of A_1 and A_2. (b) Markers with different colors represent three different amplitude sweeps. Transducers were remounted after each sweep to check the measurement error. The slope of each amplitude sweep is calculated using linear regression to obtain β. (For interpretation of the references to color in this figure legend, the reader is referred to the web version of this article.)

sweep, the measured β is a sum of system nonlinearity and material nonlinearity. We assumed system nonlinearity is constant between measurements such that any changes in β from the undeformed state come from material nonlinearity. This is the same concept as prior work studying NLU with longitudinal waves. Further, we get much better accuracy with amplitude sweep than with distance sweep because the boundary effect from the specimen geometry can be assumed constant for a fixed distance. Thus, we adopted amplitude sweep to isolate the boundary effect by fixing the measurement position.

3.3. Design considerations

We used two custom-made ultrasonic fixtures to constrain the position of the transducers and achieve a high level of precision in the measurements (Fig. 2 (a)). To determine the angle of the ACT fixture, we found the angle where β is the maximum instead of using the theoretical value, i.e., $\sin^{-1}\left(c_{air}/c_{Rayleigh}\right)$. The angle is 7.2degree and used instead of the theoretical value of 6.7degree. For the alignment of the transducers, a saddle-like shape was chosen while minimizing the clearance for pressure-fit to prevent slipping and rotation of fixtures. Similarly, the clearance between the wedge and the inner width of the wedge fixture was minimized for pressure fit. Once the wedge is mounted, the wedge is firmly held by the fixture without additional means to press the wedge onto a sample surface. This allowed us to control clamping force and control coupling in a very repeatable manner. We achieved 1 % standard deviation using this approach, which is not easily achieved in most cases.

For repeatable in situ Rayleigh wave measurements, two things must be considered: the location of ultrasonic fixtures (or transducers) on the specimen and the near-field distance. The fixtures must be mounted on the outside of the gauge area to avoid decoupling of fixtures during loading. In our preliminary measurements, the silicone rubber easily debonded after 1–2 % strain when the fixtures were on the gauge area. This is especially important to reduce the measurement variability from remounting the wedge. The gauge length of the tensile specimen must be determined based on Rayleigh distance to avoid the near-field effect (i.e., the fluctuation of the wave amplitude near the source). Rayleigh distance, x_0, for SS 316L and the frequency used (2.075 MHz-4.15 MHz) is 87.5 mm and the near-field distance is 38 mm ($0.435x_0$) [29]. The gauge length was designed to be 70 mm, considering the size of ultrasonic fixtures and the extensometer.

3.4. Measurement procedures for in situ measurements of β

During in situ ultrasonic measurements, a specimen is mounted vertically in the load frame. We do not expect orientation to affect second harmonic generation or wave propagation in the sample. However, orientation may affect measured β by changing coupling between the transducer-wedge interface over time (i.e., couplant leakage due to gravity). We measured the time dependence of β in the vertical and the horizontal orientations of the wedge to check the effect of time and orientation on the wedge-transducer coupling (Fig. 4). Based on the result, the optimal procedure is to wait 40 min after the wedge-transducer assembly is mounted in the load frame.

The actual in situ β measurements involves multiple steps: first, we glued the two fixtures to the specimen with silicone rubber, and pre-compressed them with C-clamps to cure for at least 12 h. These fixtures were designed to hold the ACT and the wedge. This sample-fixture assembly was then mounted in the load frame as shown in Fig. 2(c) and waited 40 min. Next, we prepared wedge-specimen coupling by applying a gel couplant (Olympus D12) to the bottom of the wedge. Note that the gel couplant between the specimen and wedge was chosen to minimize couplant leakage due to gravity, while an oil couplant was used to couple the transducer-wedge interface to optimize ultrasonic energy transfer. The wedge was then *pressed fit* inside the fixture (left assembly in Fig. 2(b)) and compressed on the top manually to remove any empty space. The excessive couplant around the wedge front was carefully cleaned with a brush. While the transmitting transducer remained mounted on the wedge during the entire tension test, the wedge was remounted after each amplitude sweep. While this can cause variation in coupling condition and thus variation in the measurements, our repeated measurements show a measurement error of <1 % (see

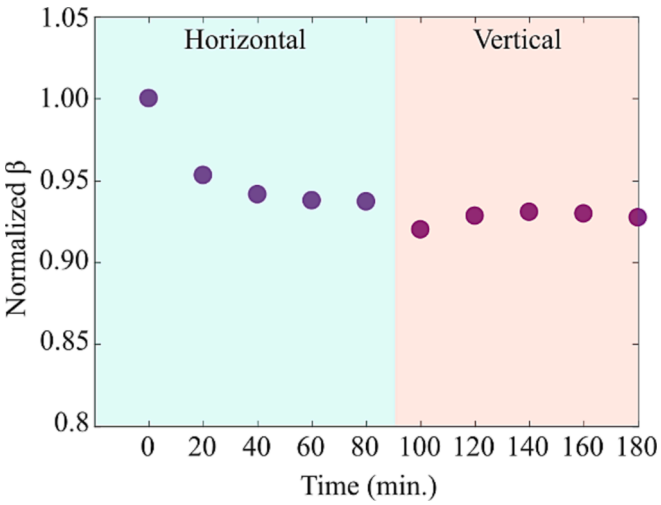

Fig. 4. The dependence of β on time and orientation. Transducers and the wedge were mounted only once for the first measurement (0 min.) and left untouched in the following measurements. Note that the specimen was initially horizontal (as shown in in Fig. 2(b)), then physically rotated 90degrees such that it was oriented vertically.

Section 4). This indicates that the change in coupling condition is negligible.

Lastly, we observed a 0.2–0.3 % increase in total strain while the specimen is held at a given stress level, i.e., room temperature (RT) creep. However, RT creep seems to happen rapidly right after holding the load for ultrasonic measurements [30]. The change of dislocation substructures due to creep during ultrasonic measurements is not significant enough to influence the NLU measurements. Fig. 5 shows that the amplitudes of A_1 and A_2 measured right after the initial amplitude sweep (~5min.) did not change much compared to those measured in the initial amplitude sweep. The difference in β between the initial amplitude sweep (black markers) and the modified amplitude sweep (the last two black markers replaced with red markers) is only 0.5 %, which is significantly smaller than the changes due to different stress levels. The strain drop can be avoided by running strain-controlled tests, but then there would be stress-relaxation instead (i.e., a decrease in stress while strain is held) [30]. Thus, stress-controlled tests are still better to study the effect of the applied stress on β at room temperature, which is the aim of this work. Similarly, a decrease in strain (elastic recovery) is observed after unloading. However, we did not observe a significant change in β after elastic recovery, presumably because the process is elastic.

4. Results

Fig. 6 shows the dependence of β on plastic strain in the unloaded configuration (0 MPa); note these measurements were conducted while the specimen was mounted in the load frame. Measurements show that in the undeformed state, β is about 2.45, and it decreases rapidly to 1.77 at 1.30 % plastic strain, followed by a saturation of β upon further plastic deformation to 5.7 % plastic strain. Three amplitude sweeps were repeated at each value of plastic strain at 0 MPa to check measurement repeatability. As indicated by small error bars on Fig. 6(a), the average standard deviation of our measurements is <1 %. In Fig. 6(b), additional data points are plotted at each stress–strain condition as shown by the markers in Fig. 1. The data points slightly deviate from the trend shown in Fig. 6(a) below 1.8 % total strain (blue and dark orange circles), and do not alter the trend above 1.8 % total strain (yellow and purple circles). The vertical deviation of data points from the red dotted line represents the effect of the applied stress. Below 1.8 % total strain, the vertical difference is more significant than that above 1.8 % total strain, which implies β is more sensitive to the applied stress at low plastic strain. The trend of decreasing β is particularly noteworthy, as all prior studies report that β increases with plastic strain [2,5,21,24,31,32], which is in contrast to our results, both in situ during loading and at 0 MPa load.

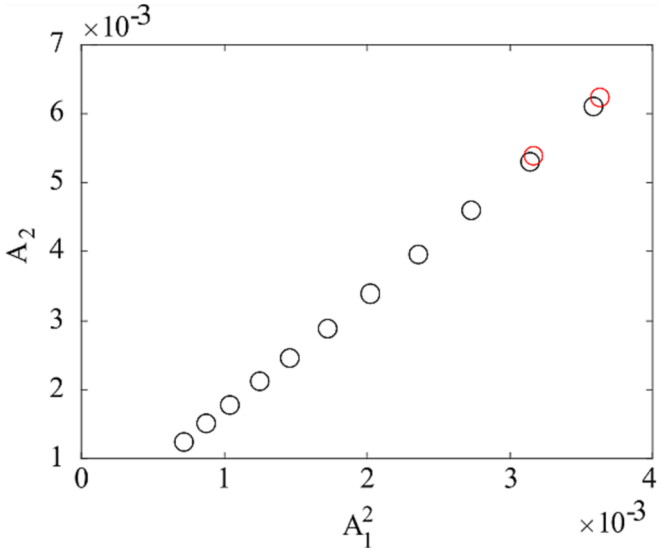

Fig. 5. A representative in situ measurement. To check the effect of RT creep on the ultrasonic measurements, two additional data points (red) were collected after one amplitude sweep (black). The difference between β was calculated from the initial amplitude sweep (11 black markers) and the modified amplitude sweep (9 black + 2 red markers) to quantify the effect of creep. The difference is only 0.5 %, which is smaller than the measurement variation (<1%). (For interpretation of the references to color in this figure legend, the reader is referred to the web version of this article.)

To study the effect of the applied stress during elastic deformation, measured β was plotted against the applied stress normalized by yield stress (Fig. 7). For small plastic strain (0 % and 0.72 %), β is more sensitive to the applied stress in the elastic regime; β increases then decreases at 0 % plastic strain, and β decreases with the applied stress at 0.72 % plastic stain. For larger plastic strain (1.3 % and 3 %), β is relatively insensitive to the applied stress below the yield stress regardless of the amount of pre-deformation. The dependence of β on the applied stress during elastic deformation can be quantified in terms of the slope of β as a function of applied stress. The slope of β is −0.0479 (blue) and −0.0853 (dark orange) for 0 % and 0.72 % plastic strains, and −0.0058 (yellow) and 0.0138 (purple) for 1.3 % and 3 %, respectively. Compared to smaller plastic strain, the slopes of β for 1.3 % and 3.0 % plastic strains are smaller and closer to zero, implying that β is more sensitive to the applied stress in early plastic deformation. These changes are not large, but they are not negligible. Further, β clearly depends on applied stress in the plastic regime, and this dependence is independent of pre-deformation. However, the dependence of β on applied stress beyond yield is also coupled to the dependence of β on plastic strain.

5. Discussion

The results in Fig. 6 and Fig. 7 highlight three aspects of the evolution of β in stainless steel 316L: β is relatively insensitive to the applied stress during elastic deformation compared to plastic deformation, β decreases with plastic deformation, and β saturates at a particular plastic strain. To interpret these results, this section discusses theoretical models and prior work.

5.1. The effect of applied stress on β

To explain the effect of applied stress on β, we need to understand the theoretical models. In Eqs. (3) and (4), the back stress is the only parameter that changes β during elastic deformation. The changes to dislocation parameters (Λ, L, and h) during elastic deformation are negligible; thus, an increase in applied stress would only increase the back stress, which will change β in the same manner as in the previous plastic deformation. In other words, the trend of β during the reloading (elastic deformation) is determined by the changes in β during the previous plastic deformation. For example, in Fig. 7, β decreases during early plastic deformation (blue markers, normalized stress > 1). When the specimen was reloaded from 0.72 % plastic strain (dark orange markers, normalized stress < 1.1), β decreases in the elastic regime. Similarly, if β saturates during plastic deformation as shown for 1.3 % or 3.0 % plastic strain in Fig. 6(b) and Fig. 7 (yellow and purple markers), β would not change much during the subsequent reloading. The changes to the slope of β in the elastic regimes shown in Fig. 7 support this argument. When β decreases with plastic deformation (0 % and 0.72 % plastic strain) the magnitude of the slopes of β during the subsequent elastic deformation are an order of magnitude larger than when β remains constant with plastic deformation (1.3 % and 3 % plastic strain), where the slopes are closer to zero in the elastic range.

5.2. Interpretation of decreasing β based on theoretical models

The results in Fig. 6 contrast those reported in prior work (e.g.,

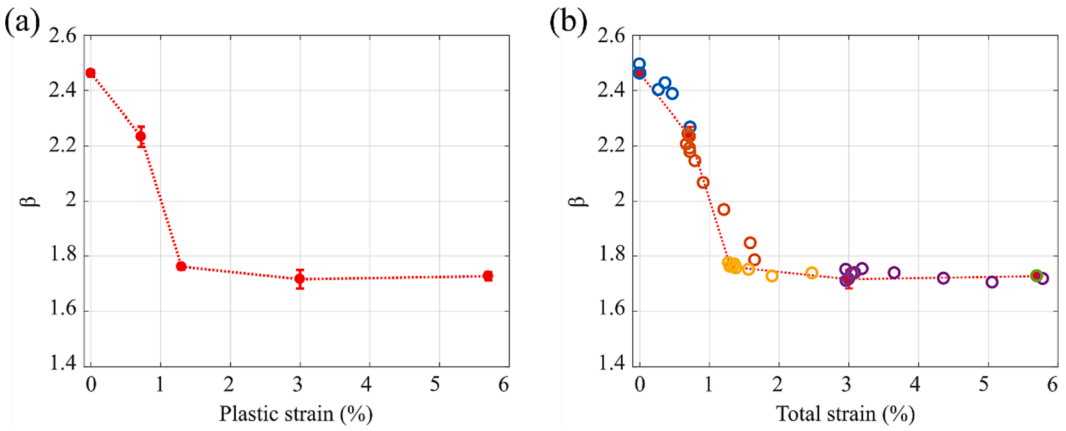

Fig. 6. (a) Dependence of β on plastic strain at 0 MPa. Three repeated measurements of β were made at 0 MPa (see Fig. 1) to check the standard deviation. The average of the standard deviations is < 1 %, which confirms the measurements are sufficiently repeatable. (b) The dependence of β on total strain at all stress levels tested plotted in addition those at 0 MPa from Fig. 6(a). β saturates after 1.8 % total strain (or 125 % yield stress). Each color represents the loading path shown in Fig. 1.

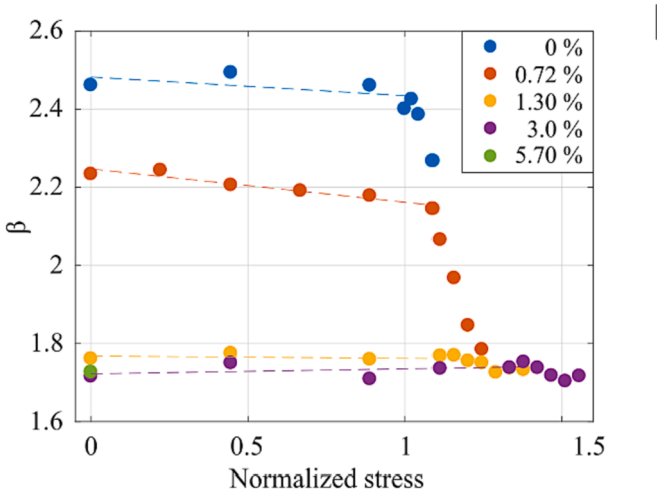

Fig. 7. Dependence of β on applied stress at different initial levels of plastic strain. Each color represents a different loading path as shown in Fig. 1, and corresponds to the accumulated plastic strain before loading (or reloading). The applied stress is normalized by the yield stress (225 MPa). β is relatively insensitive to the applied stress in the elastic regime, rapidly decreases in the early plastic regime, and saturates around 1.3 % plastic strain. The dashed lines represent the least squares regression of β measured during elastic deformation to the linear function.

[2,5,21,24,31,32]): β clearly *decreases* with increasing plastic strain. Decreasing β can be understood based on theoretical models developed by Cantrell [2]. The initial decrease in β with increasing plastic strain can be due to a competition between dislocation parameters. According to Cantrell's model, β is linearly proportional to dislocation density, however it is also proportional to dislocation characteristic length to the fourth power (e.g., monopole loop length and dipole height). Cantrell's results [2] assumed dislocation characteristic length remained constant with increasing plastic strain. This assumption means that dislocation density dominates the changes in β, not dislocation characteristic length. Such assumption is not realistic in polycrystalline metals because both dislocation density and dislocation characteristic length depend on grain orientations as well as grain boundaries. While dislocation density monotonically increases during tensile deformation, dislocation characteristic length is known to decrease with plastic deformation [33,34] because more pinning points form and there is a greater chance of dislocation intersection due to the increased dislocation density. Thus, our results suggest that L^4 decreases at a faster rate than the increase in dislocation density in this material. Additionally, prior dislocation dynamics simulations [3,4] and dislocation pile-up model [11] suggested that β can be negative, which could be another explanation for the decrease in β [4].

The above points suggest that the initial microstructure is one factor that determines the evolution of β with initial plastic deformation. It is known that β depends on grain size [35,36], however the dependence of β on plastic deformation at different initial microstructures has not yet been studied. To test our hypothesis that the dependence of β on plastic strain depends on the initial microstructure, we compare our in situ NLU measurements from Figs. 6-7 to two other specimens subjected to different heat treatments (Fig. 8). All specimens were machined from the same batch of material, and each had an "as-received (AR)" heat treatment of hot-rolling at 1100C followed by water quenching. Fig. 8 compares (1) the specimen presented in Figs. 6-7 that had a heat treatment of an additional solution annealing (SA) at 1100C for 1 h followed by *water quenching* (WQ), i.e., AR + SA + WQ, (2) a specimen in the AR condition, and (3) a specimen with an additional solution

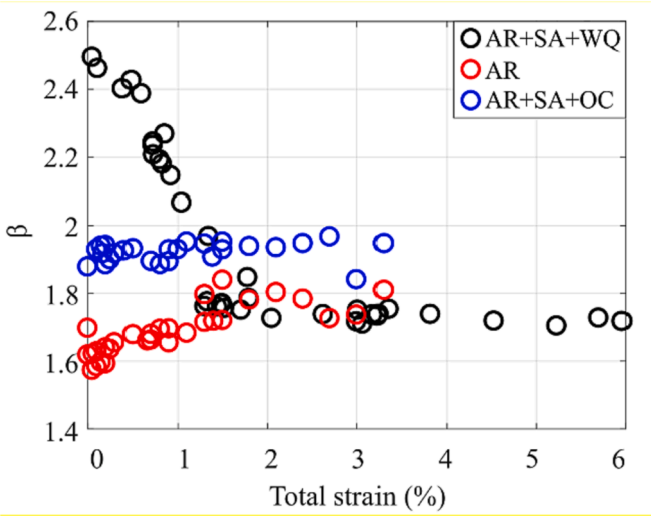

Fig. 8. The comparison of the dependence of β on total strain measured in situ, for different heat treatments: an as-received sample (AR, red), a sample with additional solution annealing and water quenching (AR + SA + WQ, black), and a sample with additional solution annealing but oven cooled (AR + SA + OC, blue). (For interpretation of the references to color in this figure legend, the reader is referred to the web version of this article.)

annealing (SA) at 1100C for 1 h but *oven cooled* (OC), i.e., AR + SA + OC. These heat treatments were selected to induce different grain sizes and phases. Specifically, the average grain size in the as-received specimen is expected to be smaller than that in the specimens subjected to additional solution annealing as shown by a decrease in yield stress from 425 MPa (AR) to 225 MPa (AR + SA + WQ). The average grain size is inversely proportional to yield stress as described by the Hall-Petch relationship [37]. The specimen subjected to oven cooling (AR + SA + OC) is expected to have σ-phase (precipitate forming between 600 and 1000C in austenitic steels) [38], which will not be present when specimens are rapidly cooled as in the water quenched samples [38]. The measurement results in Fig. 8 show strikingly different trends of β with increasing plastic strain: the AR sample shows a small increase in β (about + 12.5 %) with plastic strain, the AR + SA + WQ sample shows a decrease in β (about −30 %), and the AR + SA + OC sample shows β increases by a very small amount (about 2 %). The results in Fig. 8 support our hypothesis that the evolution of β with tensile load strongly depends on the initial microstructure.

5.3. Contrast to other work relating β to plastic strain

The measured decrease in β with plastic strain in Fig. 6 is in strong contrast to every other work that measured β over increasing plastic strain. β was shown to increase with plastic strain in aluminum alloy [39], SS 304 [40], Ni alloy [21], Ti alloy [32], AZ31 Mg-Al alloy [10], and X52 carbon steel [28]. It is typically assumed that β increases during tensile deformation, and our results provide important insight that this is not always the case. Fig. 8 show that these contrasting results may be due to the differences in initial microstructures, such as precipitates, secondary phase, and grain size. These features contribute to the characteristic lengths of edge monopoles, dipoles, and pile-ups, all of which also have competing effects on β. Similarly, dislocation evolution will be completely different depending on the material composition, slip mode (wavy or planar), and ease of cross slip.

For example, precipitates serve as pinning sites, which decrease L and thus decrease β. Similarly, grain size affects L by producing more pinning sites (i.e., grain boundaries) and by enhancing dislocation interactions near grain boundaries [34,41]. In the vicinity of grain boundaries, multiple slips occur to accommodate the intergranular strain incompatibility. Such dislocation interactions produce immobile dislocations, which are additional source of pinning sites. Grain size could affect dislocation interactions by providing/reducing preferential sites (grain boundary vicinity) for dislocation interactions.

However, why the specific material and heat treatment probed in Fig. 6 exhibit decreasing β remains a question. Compared to prior work reporting increasing β on Ni alloy [21] (planar-slip), aluminum alloy [39] (wavy-slip), X52 pipeline steel (ferrite-pearlite) [28], and SS 304 [40] (similar composition), SS316L is a one-phase material (austenite) and precipitates are not expected from solution annealing and water-quenching. These differences in initial microstructures may lead to decreasing β. Unfortunately, the link between the initial microstructure and the evolution of β during plastic deformation has received very little attention, and many studies do not provide details on heat treatment or initial microstructure. Further studies on the relationship between initial microstructure (e.g., grain size) and the evolution of β and characterizing dislocation parameters using TEM could help explain the mechanism of decreasing β.

One last point to note is the magnitude of the change in β. For example, work by Shui et al. [10] and Pfeifer et al. [28] measured changes in the magnitude of β on the order of 60–100 % over the initial 2 % strain. However, our measurements (Fig. 8) show the magnitude of β changes anywhere from 2 to 30 % over the same strain. As stated above, our results suggest that the initial microstructure strongly affects how dislocation density and dislocation characteristic length change with plastic deformation, which determines whether β increases or decreases and to what magnitude. In the work by Shui et al. [10], the initial microstructure of AZ31 Mg-Al alloy was not reported. Pfeifer et al. [28], reported that X52 pipeline steel has ferrite-pearlite structure, whose crystal structure and mechanical properties are different than austenitic steel (SS316L). Thus, a direct comparison between different materials is not feasible with the information available, which is likely why the change in β is different in our work compared to other measurements for similar strain.

5.4. The saturation of β

The final important result in Fig. 6 is the saturation of β at 1.8 % strain. The rapid transition from the linear decrease (<1.8 % strain) to the saturation (>1.8 % strain) implies a significant change in dislocation substructure around this value of plastic strain. Feaugas reported that decreasing fractions of typical planar dislocations such as stacking faults and pile-ups coincides with the onset of multiple slips at 1.5 % plastic strain in SS316L. Those planar dislocations transform to wavy-type dislocation structures such as edge dipoles, multipoles and tangles in SS 316L because of enhanced cross slip activity of screw dislocations due to multiple slip [22]. Among these wavy-type dislocations, edge dipoles and multipoles start to develop from the initial plastic deformation. At the time of the transition from planar to wavy slip, edge dipoles are observed in most grains and typical wavy-type dislocations such as tangles and walls are also formed. The constant β at higher plastic strains can be associated with the evolution of tangles and walls into cells. While we did not characterize dislocation structures in our specimen, it seems the dramatic transition in the trend of β from a monotonic decrease to saturation is associated with the transition from planar to wavy slip.

The saturation of β is also material dependent. For example, β exponentially increases with plastic strain in SS 304 [40], aluminum alloy [39], AZ31 Mg-Al alloy [10] while β saturates in Ni alloy [5] and SS 316L studied in this work. Whether β saturates with plastic deformation is particularly important as it implies a state where damage (i.e., plastic strain) continues to accumulate while β remains constant. However, the saturation of β and corresponding dislocation parameters have not been thoroughly studied.

6. Conclusions

In this work, we developed an in situ Rayleigh wave measurement setup to understand the effect of the applied stress on the evolution of β during plastic deformation. Using systematic procedures and custom-made fixtures, we were able to achieve repeatable in situ measurements, with maximum error of 1 %. For in situ NLU Rayleigh wave measurements, a SS316L dog-bone specimen was incrementally loaded up to 6 % total strain. The test was interrupted at given stress levels while loaded for ultrasonic measurements. The result shows that β is relatively insensitive to the applied stress during elastic deformation and decreases with plastic strain. The apparent stress-insensitivity of β was attributed to the competing effects between different dislocation configurations. Our results show that β decreases with plastic deformation, which was not reported previously. We attribute this trend to the differences in initial microstructure. If the initial characteristic length of dislocation structures, L, is sufficiently large from the heat treatment or manufacturing process, which is likely the case for this study, the negative contribution of β is stronger and decreases β. Alternatively, β could also decrease depending on the scaling of L during plastic deformation without relying on the negative β. Follow-up measurements on samples with different heat treatments show that the trend of β over plastic strain strongly depends on the initial microstructure. Lastly, β saturated after 1.8 % strain, which we posit is associated with the transition from planar slip to wavy slip. This work highlights three new aspects of the evolution of β during tensile deformation: (1) the effect of the applied stress, (2) decreasing β with increasing plastic strain accumulation, and (3) the saturation of β with plastic strain. Further, the in

situ NLU measurement setup and the procedures developed in this work will enable a more comprehensive understanding of how β evolves in different materials over different damage mechanisms.

CRediT authorship contribution statement

Changgong Kim: Methodology, Investigation, Formal analysis, Validation, Writing – original draft. **Kathryn H. Matlack:** Conceptualization, Supervision, Writing – review & editing.

Declaration of Competing Interest

The authors declare the following financial interests/personal relationships which may be considered as potential competing interests:

Changgong Kim reports financial support was provided by National Science Foundation.

The remaining author declare that they have no known competing financial interests or personal relationships that could have appeared to influence the work reported in this paper.

Data availability

Data will be made available on request.

Acknowledgements

This material is based upon work supported by the National Science Foundation under Grant No. CMMI-20-15599. Experimental measurements were carried out in part in the Advanced Materials Testing and Evaluation Laboratory, University of Illinois at Urbana-Champaign.

References

[1] A. Hikata, C. Elbaum, Generation of ultrasonic second and third harmonics due to dislocations. I, Phys. Rev. 144 (2) (1966) 469–477.
[2] J.H. Cantrell, Substructural organization, dislocation plasticity and harmonic generation in cyclically stressed wavy slip metals, Proc. R. Soc. A Math. Phys. Eng. Sci. 460 (2043) (2004) 757–780.
[3] W.D. Cash, W. Cai, Dislocation contribution to acoustic nonlinearity: The effect of orientation-dependent line energy, *J. Appl. Phys.* 109 (1) (2011).
[4] W.D. Cash, W. Cai, Contribution of dislocation dipole structures to the acoustic nonlinearity, *J. Appl. Phys.* 111 (7) (2012).
[5] J. Herrmann, J.Y. Kim, L.J. Jacobs, J. Qu, J.W. Littles, M.F. Savage, Assessment of material damage in a nickel-base superalloy using nonlinear Rayleigh surface waves, *J. Appl. Phys.* 99 (12) (2006).
[6] J. Zhang, F.Z. Xuan, Y. Xiang, P. Zhao, Effects of cyclic and monotonic deformations on nonlinear ultrasonic response of austenitic stainless steel: a comparative study, J. Mater. Eng. Perform. 25 (5) (2016) 2008–2016.
[7] J.-Y. Kim, L.J. Jacobs, J. Qu, J.W. Littles, Experimental characterization of fatigue damage in a nickel-base superalloy using nonlinear ultrasonic waves, J. Acoust. Soc. Am. 120 (3) (2006) 1266–1273.
[8] V.M. Rodríguez-Herrejón, A. Ruiz, C. Rubio-González, V.H. López-Morelos, J. Y. Kim, L.J. Jacobs, Nonlinear surface wave measurements on aged and laser shock surface-treated Inconel 718 superalloy, *NDT E Int.* 121 (January) (2021).
[9] C. Doerr, J.Y. Kim, P. Singh, J.J. Wall, L.J. Jacobs, Evaluation of sensitization in stainless steel 304 and 304L using nonlinear Rayleigh waves, *NDT E Int.* 88 (August 2016) (2017) 17–23.
[10] G. Shui, Y.S. Wang, F. Gong, Evaluation of plastic damage for metallic materials under tensile load using nonlinear longitudinal waves, NDT E Int. 55 (2013) 1–8.
[11] X. Gao, J. Qu, Contribution of dislocation pileups to acoustic nonlinearity parameter, *J. Appl. Phys.* 125 (21) (2019).
[12] G. Kim, C.W. In, J.Y. Kim, K.E. Kurtis, L.J. Jacobs, Air-coupled detection of nonlinear Rayleigh surface waves in concrete - Application to microcracking detection, NDT E Int. 67 (2014) 64–70.
[13] G. Kim, G. Loreto, J.Y. Kim, K.E. Kurtis, J.J. Wall, L.J. Jacobs, In situ nonlinear ultrasonic technique for monitoring microcracking in concrete subjected to creep and cyclic loading, Ultrasonics 88 (2018) 64–71, https://doi.org/10.1016/j.ultras.2018.03.006.
[14] S.C. Roy, S. Goyal, R. Sandhya, S.K. Ray, Low cycle fatigue life prediction of 316 L (N) stainless steel based on cyclic elasto-plastic response, Nucl. Eng. Des. 253 (2012) 219–225.
[15] M.S. Pham, S.R. Holdsworth, K.G.F. Janssens, E. Mazza, Cyclic deformation response of AISI 316L at room temperature: mechanical behaviour, microstructural evolution, physically-based evolutionary constitutive modelling, Int. J. Plast. 47 (2013) 143–164.
[16] J.H. Cantrell, W.T. Yost, Acoustic nonlinearity and cumulative plastic shear strain in cyclically loaded metals, *J. Appl. Phys.* 113 (15) (2013).
[17] J.H. Cantrell, Quantitative assessment of fatigue damage accumulation in wavy slip metals from acoustic harmonic generation, Philos. Mag. 86 (11) (2006) 1539–1554.
[18] T.M. Apple, et al., Acoustic harmonic generation from fatigue-generated dislocation substructures in copper single crystals, Philos. Mag. 93 (21) (2013) 2802–2825.
[19] H. Mughrabi, Dislocation wall and cell structures and long-range internal stresses in deformed metal crystals, Acta Metall. 31 (9) (1983) 1367–1379.
[20] J. Zhang, F.Z. Xuan, Fatigue damage evaluation of austenitic stainless steel using nonlinear ultrasonic waves in low cycle regime, J. Appl. Phys. 115 (20) (2014) 1–8.
[21] R.K. Oruganti, et al., Quantification of fatigue damage accumulation using nonlinear ultrasound measurements, Int. J. Fatigue 29 (9–11) (2007) 2032–2039.
[22] X. Feaugas, On the origin of the tensile flow stress in the stainless steel AISI 316L at 300 K: Back stress and effective stress, Acta Mater. 47 (13) (1999) 3617–3632.
[23] D. Kuhlmann-Wilsdorf, C. Laird, Dislocation behavior in fatigue II. Friction stress and back stress as inferred from an analysis of hysteresis loops, Mater. Sci. Eng. 37 (2) (1979) 111–120.
[24] S.V. Walker, J.Y. Kim, J. Qu, L.J. Jacobs, Fatigue damage evaluation in A36 steel using nonlinear Rayleigh surface waves, NDT E Int. 48 (2012) 10–15.
[25] K.H. Matlack, J.Y. Kim, L.J. Jacobs, J. Qu, Review of second harmonic generation measurement techniques for material state determination in metals, *J. Nondestruct. Eval.* 34 (1) (2015).
[26] D. Torello, S. Thiele, K.H. Matlack, J.Y. Kim, J. Qu, L.J. Jacobs, Diffraction, attenuation, and source corrections for nonlinear Rayleigh wave ultrasonic measurements, Ultrasonics 56 (2015) 417–426.
[27] C. Kim, Y.S. Jetti, A.C. Dunn, K.H. Matlack, Evaluating rolling contact fatigue damage precursors with Rayleigh waves in 1060 steel, *J. Nondestruct. Eval.* 40 (4) (2021).
[28] D. Pfeifer, J.Y. Kim, L.J. Jacobs, Nonlinear Rayleigh waves to evaluate plasticity damage in X52 pipeline material, Mech. Syst. Signal Process. 143 (2020), 106794.
[29] D.J. Shull, E.E. Kim, M.F. Hamilton, E.A. Zabolotskayac, Diffraction effects in nonlinear Rayleigh wave beams, J. Acoust. Soc. Am. 97 (4) (1995) 2126–2137.
[30] E. Krempl, And experimental study of room temeprature rate-sensitivity, creep and relaxation of AISI type 304 stainless steel, J. Mech. Physi. Solids 27 (1979) 363–375.
[31] A. Viswanath, B.P.C. Rao, S. Mahadevan, P. Parameswaran, T. Jayakumar, B. Raj, Nondestructive assessment of tensile properties of cold worked AISI type 304 stainless steel using nonlinear ultrasonic technique, J. Mater. Process. Technol. 211 (3) (2011) 538–544.
[32] Y. Xiang, M. Deng, F.Z. Xuan, C.J. Liu, Effect of precipitate-dislocation interactions on generation of nonlinear Lamb waves in creep-damaged metallic alloys, *J. Appl. Phys.* 111 (10) (2012).
[33] S. Catalao, X. Feaugas, P. Pilvin, M.T. Cabrillat, Dipole heights in cyclically deformed polycrystalline AISI 316L stainless steel, Mater. Sci. Eng. A 400–401 (1–2 SUPPL.) (2005) 349–352.
[34] M.S. Pham, C. Solenthaler, K.G.F. Janssens, S.R. Holdsworth, Dislocation structure evolution and its effects on cyclic deformation response of AISI 316L stainless steel, Mater. Sci. Eng. A 528 (7–8) (2011) 3261–3269.
[35] S. Choi, J. Ryu, J.-S. Kim, K.-Y. Jhang, Comparison of linear and nonlinear ultrasonic parameters in characterizing grain size and mechanical properties of 304L stainless steel, Metals (Basel) 9 (12) (2019) 1279.
[36] W. Li, B. Chen, X. Qing, Y. Cho, Characterization of microstructural evolution by ultrasonic nonlinear parameters adjusted by attenuation factor, *Metals (Basel)* 9 (3) (2019).
[37] X. Feaugas, H. Haddou, Grain-size effects on tensile behavior of nickel and AlSl 316L stainless steel, *Metall. Mater. Trans. A Phys. Metall. Mater. Sci.* 34 A (10) (2003) 2329–2340.
[38] W.E. White, I. Le May, Metallographic observations on the formation and occurrence of ferrite, sigma phase, and carbides in austenitic stainless steels. Part II: studies of AISI Type 316 stainless steel, Metallography 3 (1) (1970) 51–60.
[39] V.V.S.J. Rao, E. Kannan, R.V. Prakash, K. Balasubramaniam, Observation of two stage dislocation dynamics from nonlinear ultrasonic response during the plastic deformation of AA7175-T7351 aluminum alloy, Mater. Sci. Eng. A 512 (1–2) (2009) 92–99.
[40] J. Zhang, S. Li, F.Z. Xuan, F. Yang, Effect of plastic deformation on nonlinear ultrasonic response of austenitic stainless steel, Mater. Sci. Eng. A 622 (2015) 146–152.
[41] A. Kundu, D.P. Field, P. Chandra Chakraborti, Influence of strain amplitude on the development of dislocation structure during cyclic plastic deformation of 304 LN austenitic stainless steel, Mater. Sci. Eng. A 762 (June) (2019), 138090.